Some aspects of electrical conduction in granular systems of various dimensions

Mathieu Creyssels, Stéphane Dorbolo, Alexandre Merlen, Claude Laroche, Bernard Castaing, Eric Falcon

EPJ manuscript No.
(will be inserted by the editor)

Some aspects of electrical conduction in granular systems of various dimensions

M. Creyssels[1], S. Dorbolo[2], A. Merlen[1], C. Laroche[1], B. Castaing[1], and E. Falcon[1,a]

[1] Laboratoire de Physique, Ecole Normale Supérieure de Lyon, CNRS UMR 5672 – 46 allée d'Italie, 69 007 Lyon, France
[2] GRASP, Physics Department, Université de Liège, B-4000 Liège, Belgium

submitted to Eur. Phys. J. E on the 2nd of November 2006

Abstract. We report on measurements of the electrical conductivity in both a 2D triangular lattice of metallic beads and in a chain of beads. In both experiments, the voltage is found to increase logarithmically with the low applied current in a good agreement with a model of widely distributed resistances in series. At high enough current, the voltage saturates due to the local welding of microcontacts between beads. The frequency dependence of the saturation voltage gives a hint on the size of these welded microcontacts. The DC value of the saturation voltage ($\simeq 0.4$ V per contact) gives a measurement of the number of welded contact carrying the current within the 2D lattice. A new measurement technique gives also access to the cartography of the current paths within the 2D lattice of beads. Both the model and the cartography show the quasi-unidimensionnal feature of the electrical conductivity in such a 2D system. For both systems, the dissipated power drives the irreversibility threshold of the voltage/current characteristics. At very low current, the characteristics are found to be non linear, the non linear part of the current being a universal power law of the voltage.

PACS. 45.70.-n Granular systems – 72.80.-r Electrical conductivity of specific materials – 81.05.Rm Porous materials; granular materials

1 Introduction

Granular materials are ubiquitous in the nature and have been extensively studied mostly since the 90's [1]. However, transport phenomena within granular media such as acoustic [2,3], thermal [4] and electrical [5] conduction are not so much addressed. For instance, the stress dependence of the electrical resistance of a granular packing still is an open question [6,7].

The electrical conduction within granular solids displays astonishing properties: insulator-metal transition [7, 8,9,10], stochastic current fluctuations [11,12,13], slow relaxations [13], percolation [14,15]. Some of these electrical properties of metallic grain assemblies can be due to the extreme sensitivity of the intergrain electrical resistance to the nature of the grain surfactant [16]. One could even suspect completely irreproducible behaviours, fully dependent on the history and minute details of the material. Curiously enough, generic and reproducible behaviours can be observed in some circumstances. This paper attempts to describe some of them, comparing also 1D linear chains and 2D lattice of beads.

[a] Present address: Matière et Systèmes Complexes, Université Paris 7, CNRS UMR 7057 – 75 013 Paris, France

2 Experimental setup

The 2D experimental setup is sketched in Fig. 1. Stainless steel beads, 8 mm in diameter (with a $\pm 4\mu$m tolerance [17]), are confined in a hexagonal cell between two horizontal plates of PTFE in order to get low friction between beads and framework. The beads are placed on a triangular lattice. The total number of beads is 2792, and the size of the lattice side is 31 beads. Three sides of the hexagon are fixed, while the other may move independently along their normal direction. The applied force on each lattice side is measured by three static force sensors. The stress can be applied either isotropically or uniaxially with the help of a feedback loop [3]. In the following, only axial stress is applied to get strong stress inhomogeneities in the lattice, and thus to get a configuration particularly sensitive to disorder. Each side of the hexagon is insulated, except both ones facing each other where the uniaxial force is applied (see Fig. 1). A DC current source is supplied to these two electrodes by a source meter (Keithley 2400) which also gives a measurement of the voltage. The current source is applied to the lattice side and not to only one bead. During a typical run, the current ($10^{-6} \leq I \leq 0.1$ A) is applied and the voltage U and the resistance R is simultaneously measured. The current is supplied during a time shorter than 1s in order to avoid possible Joule heating of continuous measurements. Similar results have

been found when repeating experiments with imposing the voltage ($10^{-2} \leq U \leq 200$ V) and measuring current and resistance.

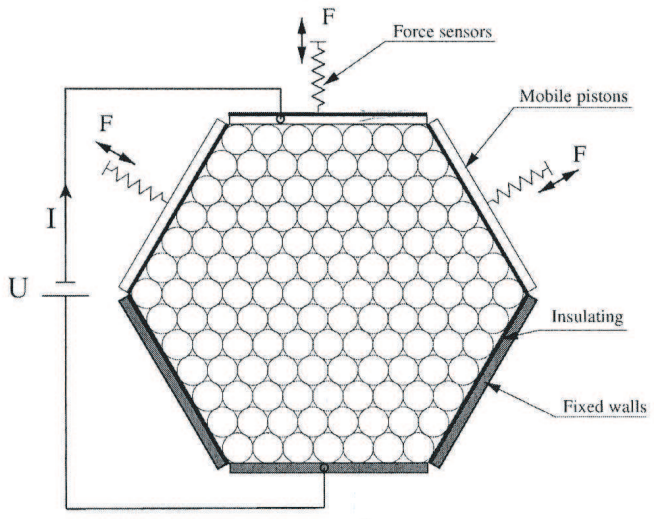

Fig. 1. Sketch of the 2D experimental setup. The real size of the lattice side is 31 beads.

In this 2D experiment, the cartography of the current paths is monitored by means of a magnetic field sensor (Bartington Inst. Mag-03) [18]. Due to the current flowing through a conductor, a magnetic field is generated perpendicularly to the axis conductor (Œrsted experiment) and is proportional to the flowing current (Biot and Savart law). The sensor range of detection is of the order of 500 μT. To avoid the Earth magnetic field detection, a high frequency (≈ 10 kHz) current is applied to the bead lattice by means of a lock-in amplifier. A typical cartography is obtained as follows. We first apply a stress and a current to the 2D lattice. The system then relaxes for one hour to avoid possible thermal drift of the current. The sensor then is moved perpendicularly to the injected current direction, from bead to bead all along each of the 60 lines of beads. In the vicinity of each bead, the value of B is then measured with the lock-in amplifier and is proportional to the current averaged on two close beads. Two hours is necessary to perform the whole current cartography.

The one-dimensional experiment consists of a chain of stainless steel beads, 8 mm in diameter (with a $\pm 4\mu$m tolerance [17]), submitted to a fixed stress. The number of beads, N, in the chain can be varied from $N = 2$ to 40. A current, I, is applied to the chain, and the voltage U of the whole chain is simultaneously measured (in the same way as in the 2D experiment) as well as the voltage, U_i, between each beads by means of multimeter/switch system (Keithley 2700 with multiplexer module 7702). The 1D experimental setup has been already described elsewhere [7].

Note that for both experiments, after each cycle in current, new contacts between each bead are needed to have reproducible measurements for the next cycle [7]. To wit, the applied force is reduced to zero, and we roll the beads which allow to form new contacts for the next cycle.

3 Voltage/current characteristics: saturation voltage

The typical electrical characteristics of a chain of beads is schematically displayed in Fig. 2 (see Ref. [7,10]). Its properties can be summarized as follows. For a given applied current I, different voltages $U(I)$ can be measured. Its value is dependant on the history of the injected current. When the current never went upper than I since the last renewing of contacts, the behaviour of the contact is called up-characteristics. On the other hand, when a larger current has been already applied, the behaviour is named down-characteristics. Down-characteristics are always reversible: as far as $|I| < I_{max}$ (I_{max} being the maximum current already applied), the relation $U(I)$ is symetric [$U(I) = -U(-I)$] and remains the same whatever the history of I since the last occurence of $I = I_{max}$.

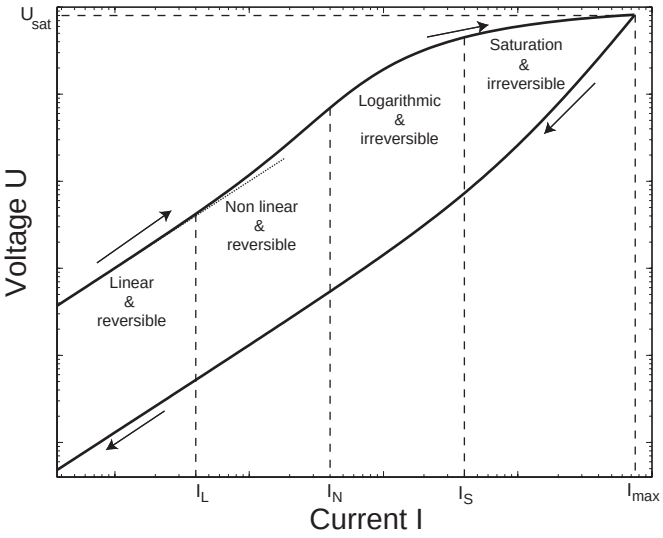

Fig. 2. Log-Log schematic view of the $U - I$ characteristics for a 1D granular medium. The currents I_L, I_N, and I_S define the limits of the different regimes of the up-characteristics (see text).

Depending of the applied force, three different characteristic currents I_L, I_N, and I_S can be defined (see Fig.2)

- If $I_{max} < I_L$, up and down-characteristics are identical and linear (see Fig. 2).
- If $I_L < I_{max} < I_N$, up and down-characteristics remain identical but are non-linear (see Fig. 2). Section 6 is particularly devoted to this range.
- For $I > I_S$, the up-characteristics shows a constant voltage U, proportionnal to the number of contacts ($U \simeq 0.4$V per contact), as shown in Fig. 3a. The down

characteristics is non linear, revealing the existence of a metallic bridge (or microwelding) between beads at each contact [7,10]. The resistance increases with the temperature of the bridge, which itself only depends on the voltage across it. This is the range we discuss in the present section.

– Finally, for $I_N < I_{max} < I_S$, up-characteristics progressively raises up to the saturation voltage (see Fig. 2). Down-characteristics are intermediate between those of the two neighbouring ranges. This will be discussed in Sec. 5.

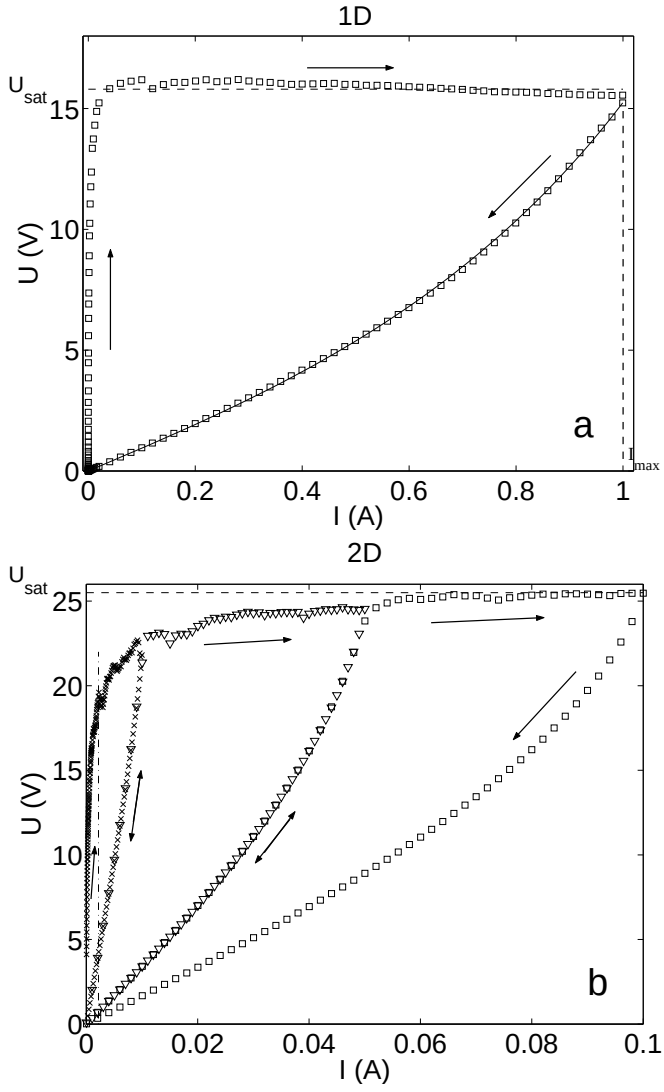

Fig. 3. Typical $U - I$ characteristics. **(a)** 1D chain of $N = 38$ beads for an applied force $F = 100$ N. The dashed line $U_{sat} \simeq 15.8$ V corresponds to a saturation voltage per contact of $V_o \equiv U_{sat}/(N+1) \simeq 0.4$ V. The solid line is the theoretical down trajectory (see Ref. [7,10]). **(b)** 2D lattice of beads for an applied force $F = 50$ N. The dashed line corresponds to the saturation voltage $U_{sat} \simeq 25.4$ V. This value gives a measurement of the number of welded contact (see text). Different symbols correspond to different maximum current applied, I_{max}.

The new results about the saturation range concern two points: the extension to 2D systems (see below) and the extension to AC voltages for the 1D system (see Sec. 4).

The $U - I$ characteristics of a chain of 38 beads is shown in Fig. 3a. Such typical curve has already been discussed in Ref. [7,10]. Figure 3b displays the electrical characteristics for the 2D lattice of beads. Qualitatively, it is the same characteristics than the 1D ones. This is quite surprisingly at first sight, but this can be understood when looking at the current map displayed on Fig. 4. This cartography shows the localization of the current in few discrete paths. To our knowledge, this is the first experimental cartography measuring the current distribution within a granular medium, at low applied voltage. Note that direct infrared visualizations and numerical simulations of temperature distribution exist [8,20], as well as various 2D models of random resistor network [21]. On Fig. 4, the current is mainly concentrated on lines which are probably reminiscent of those where stress is concentrated in such systems [19]. The contacts resistances rapidly depend on the applied force [7], which could justify this analogy, but they are also widely distributed for a given force, as will be seen later. This random distribution of resistances could also yield to the concentration of current on percolating lines [14]. Indeed, we could not identify the lines of maximum current with those of maximum stress.

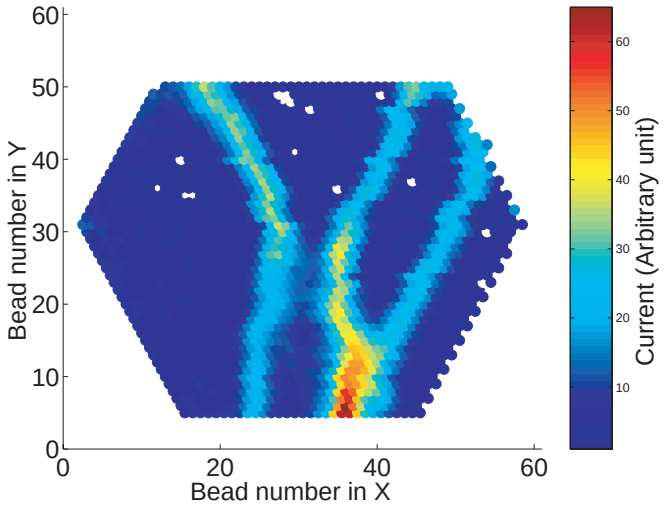

Fig. 4. Typical vizualization of the current path network in an 2D hexagonal packing of metallic beads. The size of the lattice side is 31 beads. The upper part (bead number greater than 50) has not been measured. (Color figure)

Nevertheless, the concentration of current on lines explains the similarity between the electrical characteristics in the 1D and 2D lattices. The 25.4 V saturation voltage reached for the 2D lattice (see Fig. 3b) gives a number of 64 ± 1 welded contacts when compared to the $V_o \equiv 0.4 \pm 0.01$V per contact of the 1D chain. This estimate is in good agreement with the dimensions of the hexagon (31 beads per side). Thus, as in the 1D system,

the saturation voltage is also a measurement of the number of welded contact in the 2D system.

4 Frequency dependence of the saturation voltage

Let us now examine the AC electrical response of the 1D chain. As far as the saturation voltage is concerned, two extreme cases can be considered:

- Either the contact temperature can follow the voltage variations across a contact. Then the 0.4V per contact corresponds to the peak amplitude of the AC voltage across a contact. For a sine like variation in the voltage, the rms value of the saturation voltage is then $0.4/\sqrt{2} \simeq 0.28$ V per contact. The temperature variations occur at twice the frequency of the voltage. This doubling temperature frequency stems from the dependence of the contact temperature on the square of the voltage (see below).
- Or the temperature cannot follow the voltage variations due to the specific heat of the material. Then, the 0.4 V are the rms saturation voltage across the contact.

To discuss the intermediate regime between these two extreme cases, let us introduce the influence of the specific heat in the thermal budget. We approximate the temperature T and voltage U fields as spherical around the center of the metallic bridge. Half of the Joule heating goes in each bead. The current flowing from the left to the right bead, and considering the right bead, we define u as the (negative) difference between the potential at distance r and the potential at the center. Far from the center, $T = T_o$ and $u = -U/2$. At the center ($r = 0$), $T = T(0)$ and $u = 0$. The total heat flux at distance r is

$$-\lambda 2\pi r^2 \frac{\partial T}{\partial r} \tag{1}$$

where λ is the heat conductivity. The current I is

$$I = -\frac{2\pi r^2}{\rho}\frac{\partial u}{\partial r} \tag{2}$$

where ρ is the electrical resistivity. Joule heating within the considered bead at distance less than r is then

$$-uI = \frac{2\pi r^2}{\rho}\frac{u\partial u}{\partial r}\ . \tag{3}$$

The thermal budget then writes

$$-\lambda 2\pi r^2 \frac{\partial T}{\partial r} = \frac{2\pi r^2}{\rho}\frac{u\partial u}{\partial r} - \int_0^r C 2\pi r'^2 \frac{\partial T(r')}{\partial t} dr' \tag{4}$$

where C is the specific heat of the bead material. Using the relation $\lambda\rho = LT$ (see Ref. [7,10]), where $L \simeq 2.5\,10^{-8}$ V^2/K^2 is the Lorentz number, Eq. (4) can be written as

$$T\frac{\partial T}{\partial r} = -\frac{u\partial u}{L\partial r} + \frac{T}{\lambda r^2}\int_0^r C r'^2 \frac{\partial T(r')}{\partial t} dr'\ . \tag{5}$$

Integrating Eq. (5) from $r = 0$ to ∞ gives

$$T(\ell)^2 - T(0)^2 = -\frac{u^2}{L} + \int_0^\ell \frac{2T}{\lambda r^2}\int_0^r C r'^2 \frac{\partial T(r')}{\partial t} dr' dr \tag{6}$$

or, with $T_m \equiv T(0)$,

$$T_m^2 - T_o^2 = \frac{U^2}{4L} - \int_0^\infty \frac{2T}{\lambda r^2}\int_0^r C r'^2 \frac{\partial T(r')}{\partial t} dr' dr\ . \tag{7}$$

This is the modified Kohlrausch equation due to the second term in the right-hand side of Eq. (7) taking the temporal dependence into account (see Ref. [7,10] for details on the Kohlrausch equation at the thermal equilibrium). The influence of this last term is examined in the Appendix A for a sinusoidal voltage $U = U_o \cos\omega t$. We then find

$$T_m^2 - T_o^2 = \frac{U_o^2}{8L}\left[1 + \theta(\omega)\cos(2\omega t - \phi(\omega))\right] \tag{8}$$

where

$$\theta(\omega) = \frac{1}{\sqrt{1 + G(\omega)^2}}\ ;\ G(\omega) = \frac{4a}{5}\sqrt{\frac{2\omega}{\kappa}} \tag{9}$$

$a = \rho I_o/\pi U_o$ being of the order of the radius of the metallic bridge (see Appendix A). $I = I_o \cos\omega t$ is the first (and main) harmonics of the current, κ and ϕ being introduce in Appendix A.

As explained in [7,10], the maximum value of T_m^2, is fixed to $V_o^2/4L$ by the softening of the metallic bridge, with $V_o \simeq 0.4$V. Substituting this variable into Eq. (8) leads to the rms saturation voltage

$$U_{\rm rms}^2 \equiv \frac{U_o^2}{2} = \frac{V_o^2}{1+\theta(\omega)} = V_o^2 \frac{\sqrt{1 + (32a^2\omega/25\kappa)}}{1 + \sqrt{1 + (32a^2\omega/25\kappa)}} \tag{10}$$

Defining $I_{\rm rms} \equiv I_o/\sqrt{2}$ and $A \equiv 8\rho/(5\pi V_o)$, the AC current–voltage characteristics then writes

$$U_{\rm rms}^2 = V_o^2 \frac{\sqrt{1 + (A^2 I_{\rm rms}^2\omega/\kappa)}}{1 + \sqrt{1 + (A^2 I_{\rm rms}^2\omega/\kappa)}} \tag{11}$$

Figure 5 shows a comparison between measurements at 1MHz and model of Eq. (11). The value of A used for the best fit in solid line is within 30% that obtained from the physical properties of the stainless steel corresponding to our beads [22]. V_o is given by the DC saturation measurements. The uncertainties on the measurements do not allow to claim for a full agreement. However, it is clear that the model gives the good order of magnitude for the frequency effects, and well explains the very progressive character of the saturation in such conditions. It also confirms the size of the metallic bridge explaining the saturation plateau: it is of the order of $a \simeq 50$ nm for $I = 10^{-1}$ A, and is proportional to the current I.

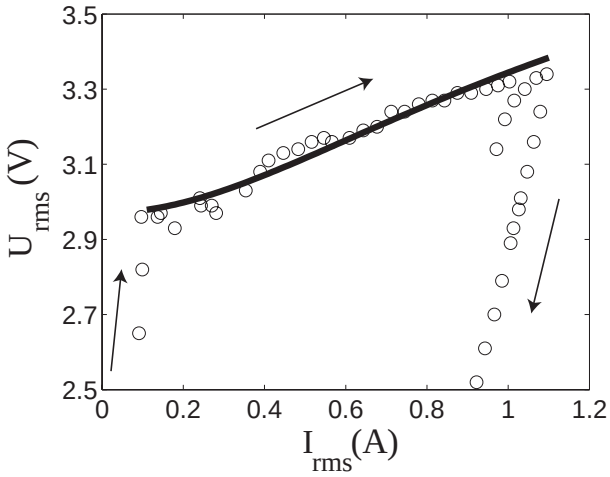

Fig. 5. Comparison between the AC characteristics measured at 1 MHz (∘) in the chain of 11 beads, and the model (−) from Eq. (11). Only the top part of the experimental curve is shown here to focus on the saturation regime.

5 Up-characteristics for $I_N < I < I_S$

Let us now focus on the intermediate range of the DC applied current $I_N < I < I_S$ (see Fig. 2). In this case, the voltage across the 1D chain of beads progressively grows up to the saturation voltage. For this current range, the characteristics of the Fig. 3a is shown in log-lin axes in Fig. 6a. It can be modelized, on roughly two decades, as

$$U \propto \ln I \ . \tag{12}$$

Only an inhomogeneity of resistances occurs between beads along the chain. In the 2D experiment, there are both stress [19] and resistance inhomogeneities. However, Fig. 6b shows that a similar logarithmic characteristics is also observed with the 2D experiment for this range of current.

We argue that it is simply due to the wide distribution of contact resistances between beads. The rough argument is as follows. When the current is progressively raised from zero, the contacts with the largest resistances reach the saturation voltage first. Consequently, a further increase of the current does not result in voltage increase for each of these contacts. On the other hand, the contacts with the lowest resistances do not contribute either to the total rise in voltage. Thus this rise is due to the contacts whose resistance is such that they are close to the saturation voltage V_o. This resistance is thus V_o/I. For a variation of current δI, their voltage increase is $\delta U = (V_o/I)\delta I$. This yields by integration to the log dependence of Eq. (12) in qualitative agreement with the observation displayed in Fig. 6.

A direct measurement of the cumulative distribution of resistances in the chain confirms this broad distribution of contact resistances between beads (see Figs. 7 and 8). Figure 7 shows, in Log-Lin axes, the typical cumulative distribution function of the total resistance of a chain of 17 beads during 480 realizations. The distribution is

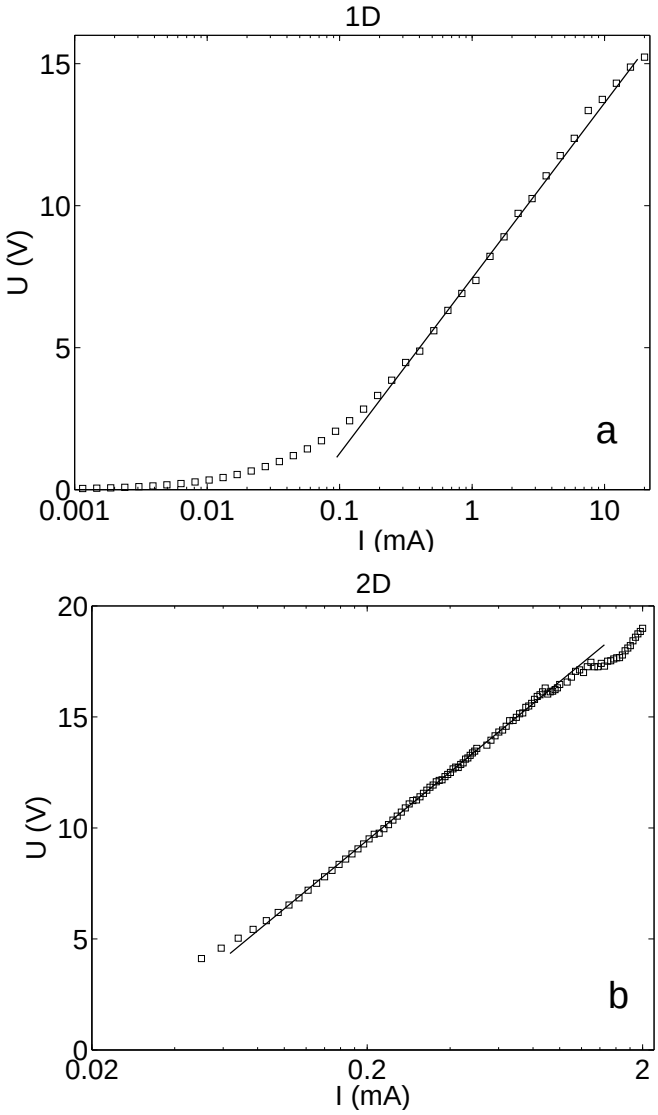

Fig. 6. Zoom of the U-I characteristics in Fig. 3 in Log-Lin axes. **(a)** 1D and **(b)** 2D experiment. (−): fits $U \propto \ln I$.

broad before the saturation regime, and narrower after the saturation. The inset of Fig. 8 shows the values of the resistance between 2 beads during 600 realizations before the saturation regime. These values are spread on more than 3 decades. The cumulative distribution function of the logarithms of resistances is well fitted (see solid line in Fig. 8) by a log-normal distribution [16,23]. Even simpler, a flat distribution in resistance logarithms is also a good model, which is equivalent to approximate the cumulative distribution of Fig. 8 by its inflexion point tangent.

Such an approximation allows to formalize the above argument. Assume that the resistances r are such that the probability density of their logarithm, $\ell \equiv \ln(r/r_o)$, is $P_o(\ell) = 1/(2\ell_m)$ for $-\ell_m < \ell < \ell_m$. This uniform distribution P_o is normalised by the constant ℓ_m, and r_o is a constant with the dimension of a resistance. Then, the

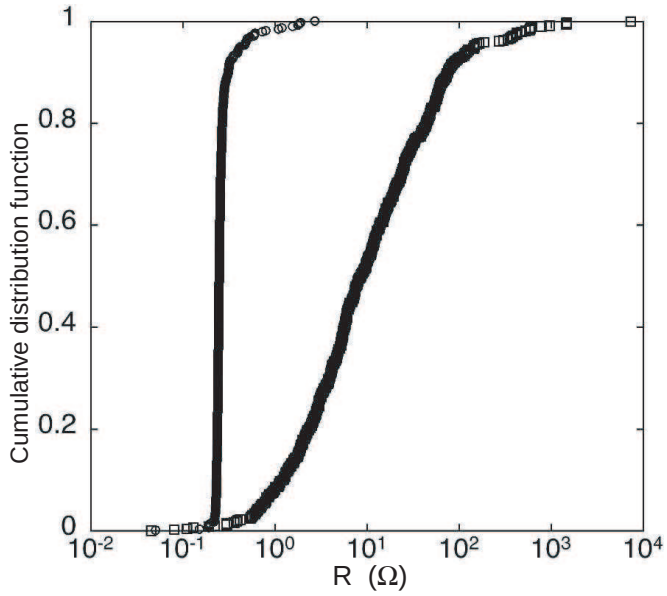

Fig. 7. Cumulative distribution function of the resistance of a chain of N=17 beads for 480 realizations (in Log-Lin axes): before (□) and after (○) the saturation regime (see Fig. 3). $\langle R \rangle$ = 38.3 Ω before (0.29 Ω after), and σ_R = 154.5 Ω before (0.22 Ω after).

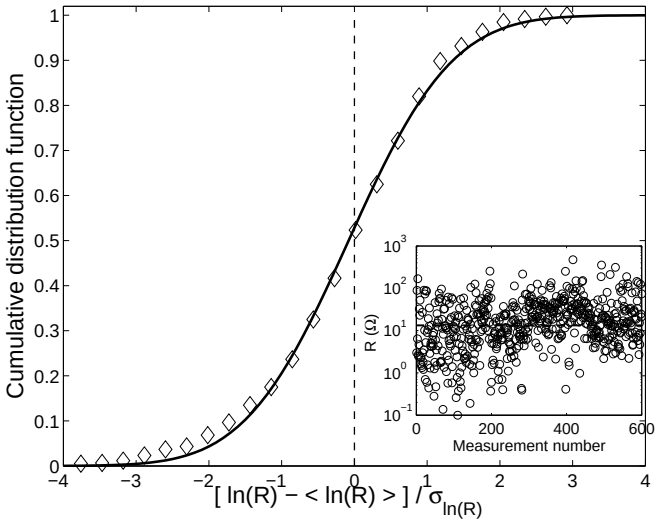

Fig. 8. Inset: values of the resistance, R, between 2 beads during 600 realizations (under stress of 200 N before the saturation regime). $\langle R \rangle$ = 28 Ω ; σ_R = 43 Ω ; $e^{\langle ln(R) \rangle}$ = 13 Ω (−−), and $\sigma_{ln(R)}$ =1.16. Main: Cumulative distribution function of $ln(R)$ (centered to the mean and normalised by the rms value). Solid line is a Log-normal fit of mean -0.08 and standard deviation 1.12.

average voltage per contact is

$$U = r_o I \int_{-\ell_m}^{\ln\left(\frac{V_o}{r_o I}\right)} P_o e^{\ell} d\ell + V_o \int_{\ln\left(\frac{V_o}{r_o I}\right)}^{\ell_m} P_o d\ell$$

and

$$\frac{dU}{dI} = r_o \int_{-\ell_m}^{\ln\left(\frac{V_o}{r_o I}\right)} P_o e^{\ell} d\ell = r_o P_o \left(\frac{V_o}{r_o I} - e^{-\ell_m} \right)$$

As $(V_o/r_o I) >> e^{-\ell_m}$, we find $dU/dI = P_o V_o / I$ which leads to the expected logarithm characteristic. Figure 7 also shows that, once the saturation voltage is reached, all resistances have the same value V_o/I_{max} (see also [24]).

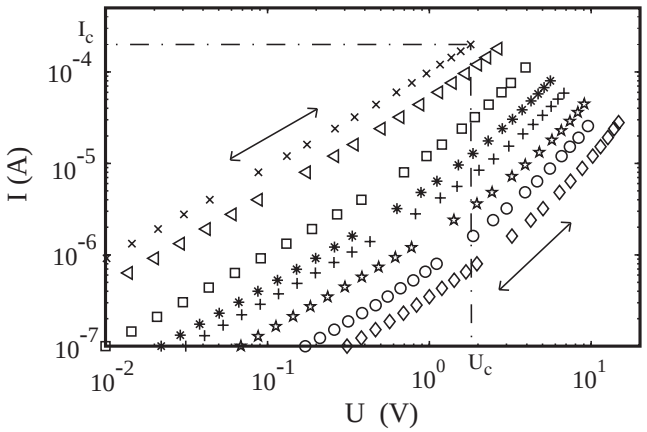

Fig. 9. Non linear reversible characteristics. The characteristics are reversible up to the point (U_c, I_c). Different symbols correspond to different applied forces. 1D experiment with $N = 40$.

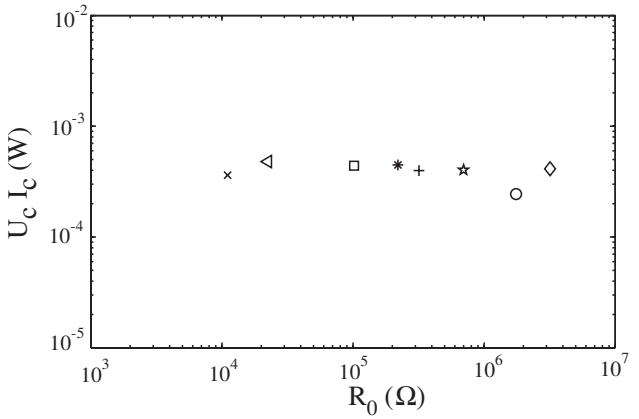

Fig. 10. Critical power $U_c I_c$ (for which the characteristics of Fig. 9 become irreversible) as a function of R_0. R_0 is the value of the chain resistance at low applied current. Same symbols as Fig. 9.

6 Non linear reversible characteristics

We now examine the part of the characteristics corresponding to $I_L < I < I_N$ (see Fig. 2). While capturing

the main origin of the $\ln I$ behaviour for $I_N < I < I_S$, the model of the previous section is oversimplified. It suggests that the characteristics is linear up to the point where the contact with the largest resistance reaches 0.4V. This is not true. Figure 9 shows that non linearities appear while the characteristics remains reversible.

Different applied forces, or even different experiments at the same force, yield to different values for the irreversibility threshold (see Fig. 9). However, as shown on Fig. 10, the dissipated power $U_c I_c$ at the irreversibility threshold has approximately the same value $P_c = U_c I_c$ for a very wide range of initial resistances R_o, at least for a fixed number of contacts. Similar power dependent threshold has recently been reported for 3D samples of copper powder [12,13]. However, here, we do not observe any time evolution of the resistance once the threshold exceeded, as was the case in these 3D samples. While the influence of the dissipated power suggests a thermal origin, we have no precise model for this threshold.

In order to characterize the non linearity, we plot $R_o I - U$ versus U on Fig. 11, that is, the non linear part of the current, normalised by the initial resistance at low applied current, R_0. The logarithmic plot stresses the power law behaviour of this non linear part

$$R_o I - U = U_a \left(\frac{U}{U_a} \right)^{\alpha} \tag{13}$$

where U_a is the amplitude of this non linear part of the current. U_a cannot apparently be considered as universal, even at constant number of contacts, depending of the experiment without clear correlation with the applied force. However, α is always found close to $2.3 \simeq 7/3$. Note that, for 3D copper powder samples, a similar non linear behaviour was observed [12], for which a different formula was proposed

$$R_o I - U = c R_o I (UI)^{1/2}$$

c being a constant. However, this above formula leads to

$$\alpha = \frac{\partial \ln(R_o I - U)}{\partial \ln(U)} = \frac{1}{2} + \frac{3}{2} \frac{\partial \ln(I)}{\partial \ln(U)} > 2$$

in qualitative agreement with the present results.

The situation for 3D copper powder samples will be clarified in [25]. Let us add a few comments about the interplay between the irreversibility threshold occuring at a constant dissipated power (P_c), and the saturation threshold ($U = 0.4$V per contact). At the former one, $U^2 < R_o P_c$, which means that, for sufficiently small initial resistance R_o, it will occur before the saturation. However, for large enough R_o (small applied forces), it should occur after. This is impossible, as our explanation of the saturation implies the irreversibility. Indeed, in such situations, we observed that the voltage U can cross the saturation value, and continue to grow until the irreversibility occurs.

7 Conclusion

To conclude, the experimental results reported here allow both to confirm previous interpretations and to raise new questions. The dependence of the saturation voltage with the frequency confirms the model of the metallic bridge, including the order of magnitude of its size. Both the characteristics and the cartography of the current paths within the 2D lattice show the quasi-unidimensionnal feature of the electrical conductivity in such 2D systems. The inhomogeneity of the oxyde layer at the surface of the beads reflects in a wide distribution of contact resistances. This wide resistance distribution results in a logarithmic behaviour for the $U - I$ characteristics, a further example of how disorder can induce universal laws. On the other hand, an extension of this work is to understand the non-linear reversible behaviour observed at low current. The most remarkable feature it presents is the apparent universality of the non conventionnal exponent α.

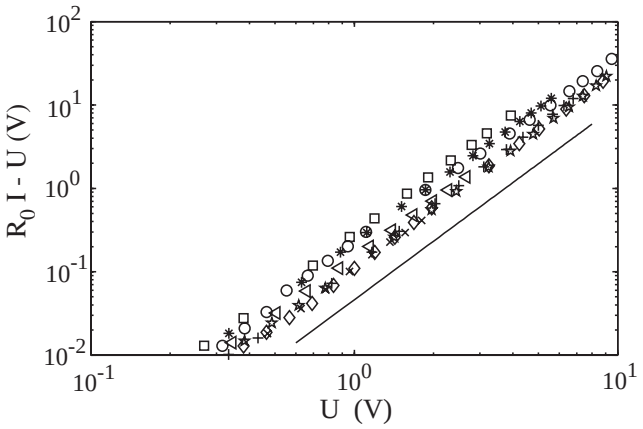

Fig. 11. Normalised non linear part of the current as a function of the voltage U. The logarithmic slope is close to $2.33 \simeq 7/3$. Same symbols as Fig. 9.

A part of this work was supported by the French Ministry of Research under Grant ACI Jeunes Chercheurs 2001. S. Dorbolo is an FNRS research associate, and gratefully acknowledges the hospitality of the Physics Laboratory at the ENS Lyon. We thank J.-F. Pinton and H.-C. Nataf for lending us the magnetic field sensor.

Appendix A

Our goal is to approximately solve the Kohlrausch modified equation (7)

$$T(0)^2 - T_o^2 = \frac{U^2}{4L} - \int_0^{\infty} \frac{2T}{\lambda r^2} \int_0^r C r'^2 \frac{\partial T(r')}{\partial t} dr' dr \tag{14}$$

with $U = U_o \cos \omega t$.

To wit, we shall use a low frequency approximation for $T(r)$ in the integrals. The imposed voltage across the contact is $U = U_o \cos \omega t$. Thus, $u = -(U_o/2) f(r) \cos \omega t$ and $I = I_o \cos \omega t$. Substituting these two equations into Eq. (2) gives

$$I_o = \frac{U_o \pi}{\rho} r^2 \frac{\partial f}{\partial r} \ .$$

Neglecting the temperature dependence of ρ, we define $a = r^2 \partial f/\partial r$, a constant length which is of the order of the radius of the metallic bridge. As $f = 1$ for $r = \infty$, the above relation integrates as $f = 1 - (a/r)$ which is valid for $r >> a$. For $r = 0$, $f = 0$. We shall thus use the ansatz:

$$f(r) = 1 - \frac{a}{r+a} = \frac{r}{r+a}$$

Let us now limit ourselves to the first harmonics in 2ω, that is

$$T(r) = T_\infty \left[h_o(r) + \theta(\omega) h_1(r) \cos(2\omega t - \phi(\omega))\right] \qquad (15)$$

with $h_o(0) = 1$, $\phi(0) = 0$, $\theta(0) = 1$ and $\theta(\infty) = 0$.

There is several approximations here. We assume $\phi(\omega)$ is independent of r, and h_1 independent of ω. However, $\phi(\omega)$ is probably larger when r increases, as the volume of the involved material ($\propto r^3$) is larger. In the same way, $h_1(r)$ is probably smaller at large r for small ω than for large ω. Both effects have the result to effectively limit the integral to r smaller than the diffusion length. We thus take them into account by putting the upper limit in r to $\ell_D = \sqrt{\kappa/2\omega}$, with $\kappa \equiv \lambda/C$, λ being the thermal conductivity and C the specific heat of the bead material.

Within the same approximations, at low frequency, Eqs. (6) and (7) then write

$$T(r)^2 - T_o^2 = \frac{U_o^2}{8L}(1 - f^2)(1 + \cos 2\omega t)$$

$$= T_\infty^2 h_o^2 + 2T_\infty^2 h_o h_1 \cos(2\omega t) - (T_o^2 - T_\infty^2 h_1^2/2)$$

Neglecting the last term, we obtain

$$T_\infty^2 = \frac{U_o^2}{8L} \; ; \; h_o = \sqrt{1 - f^2} \; ; \; h_1 = h_o/2 \; .$$

Looking only at the 2ω terms, Eq. (14) then writes

$$\theta(\omega)\cos[2\omega t - \phi(\omega)] = \cos(2\omega t) + G(\omega)\theta(\omega)\sin[2\omega t - \phi(\omega)]$$

with

$$G(\omega) = 4\omega \int_0^{\ell_D} \frac{h_o(r)}{\lambda r^2} \int_0^r C r'^2 h_1(r') dr' dr \; ,$$

or

$$G(\omega) \simeq \frac{2\omega}{\kappa} \int_0^{\ell_D} \frac{h_o(r)}{r^2} \int_0^r r'^2 h_o(r') dr' dr \; . \qquad (16)$$

It thus gives

$$\theta(\omega) = \frac{1}{\sqrt{1 + G(\omega)^2}} \; . \qquad (17)$$

Keeping only the dominant term in Eq. (16), thus taking $h_o \simeq \sqrt{2a/r}$, that is

$$\int_0^r r'^2 h_o(r') dr' \simeq \frac{2\sqrt{2a}}{5} r^{5/2} \; ,$$

we finally obtain

$$G \simeq \frac{2\omega}{\kappa} \frac{4a}{5} \ell_D = \frac{4a}{5} \sqrt{\frac{2\omega}{\kappa}} \; .$$

References

1. *Powders and Grains 2005*, edited by R. Garcia-Rojo, H. J. Herrmann and S. McNamara (Taylor & Francis Group, London, 2005), and references therein
2. J. D. Goddard, Proc. R. Soc. Lond. A **430**, 105 (1990), C. Liu and S. R. Nagel, Phys. Rev. B **48**, 15646 (1993), C. Coste, E. Falcon and S. Fauve, Phys. Rev. E **56**, 6104 (1997); E. Falcon, C. Laroche, S. Fauve and C. Coste, Eur. Phys. J. B **5**, 111 (1998); X. Jia, C. Caroli and B. Velicky, Phys. Rev. Lett. **82**, 1863 (1999)
3. B. Gilles and C. Coste, Phys. Rev. Lett. **90**, 174302 (2003)
4. G. K. Batchelor and R. W. O'Brien, Proc. R. Soc. Lond. A **355**, 313 (1977); J.-C. Géminard, D. Bouraya and H. Gayvallet, Eur. Phys. B **48**, 509 (2005)
5. R. Holm, *Electric Contacts* 4th edn. (Springer Verlag, Berlin, 2000); R. S. Timsit, *Electrical Contacts, Principles and Applications*, Ed. P. Slade (Marcel Dekker, New York, 1999)
6. F. P. Bowden and D. Tabor, Proc. Roy. Soc. Lond. A **169**, 391 (1939); K. J. Euler, J. Power Sources **3**, 117 (1978); M. Ammi et al., J. Phys. (Paris) **49**, 221 (1988); X. Zhuang, J. D. Goddard and A. K. Didwania, J. Comp. Phys. **121**, 331 (1995)
7. E. Falcon, B. Castaing and M. Creyssels, Eur. Phys. J. B **38**, 475 (2004)
8. D. Vandembroucq, A. C. Boccara and S. Roux, J. Phys. III **7**, 303 (1997);
9. E. Branly, C. R. Acad. Sci. Paris **111**, 785 (1890) (in french); S. Dorbolo, M. Ausloos and N. Vandewalle, Phys. Rev. E **67**, 040302(R) (2003)
10. E. Falcon and B. Castaing, Am. J. Phys. **73**, 302 (2005)
11. G. Kamarinos, P. Viktorovitch and M. Bulye-Bodin, C. R. Acad. Sci. Paris **280**, 479 (1975) (in french); G. Kamarinos and A. Chovet, in *Proceed. SEE: Conducteurs Granulaires*, edited by E. Guyon (Paris, 1990), p. 181 (in french); D. Bonamy et al., Europhys. Lett. **51**, 614 (2000); N. Vandewalle, C. Lenaerts and S. Dorbolo, Europhys. Lett. **53**, 197 (2001).
12. E. Falcon, B. Castaing and C. Laroche, Europhys. Lett. **65**, 186 (2004)
13. M. Creyssels, Ph.D. thesis, Ecole Normale Supérieure de Lyon, 2006
14. V. Ambegaokar, S. Cochran, and J. Kurkijärvi, Phys. Rev. B **8**, 3682 (1973)
15. K. K. Bardhan, Physica A **241**, 267 (1997) and references therein; J. P. Troadec and D. Bideau, J. Phys. (Paris) **42**, 113 (1981) (in french)
16. V. Da Costa et al., Eur. Phys. J. B **13**, 297 (2000)
17. Marteau & Lemarié. Specialist of beads. Product Catalogue
18. See Mag-03MC Fluxgate Sensor Operation Manual in http://www.gmw.com
19. P. Dantu, Géotechnique **18**, 50 (1968) (in french); A. Drescher and G. De Josselin De Jong, J. Mech. Phys. Solids **20**, 337 (1972); T. Travers et al., J. Phys. (Paris) **49**, 939 (1988); D. W. Howell, R. P. Behringer and C. Veje, Phys. Rev. Lett. **82**, 5241 (1988)
20. J. Zhang and A. Zavaliangos, in *Granular Material-Based Technologies, MRS Proceedings Vol. 759*, edited by S. Sen, M.L. Hunt, and A.J. Hurd (MRS Fall Meeting 2002, Boston, MA, 2002)

21. A. Vojta and T. Vojta, J. Phys.: Condens. Matter **8**, L461 (1996); S. Roux and H. J. Herrmann, Europhys. Lett. **4**, 1227 (1987)
22. See AISI 304 Stainless Steel properties on the web
23. M. Evans, N. Hastings and B. Peacock, *Statistical distributions* (John Wiley & Sons, 1993)
24. S. Dorbolo, A. Merlen, M. Creyssels, E. Falcon, N. Vandewalle, and B. Castaing *Influence of electromagnetic waves on the electrical properties of a single contact between conducting grains* (in preparation).
25. M. Creyssels, B. Castaing and E. Falcon, in preparation (unpublished).